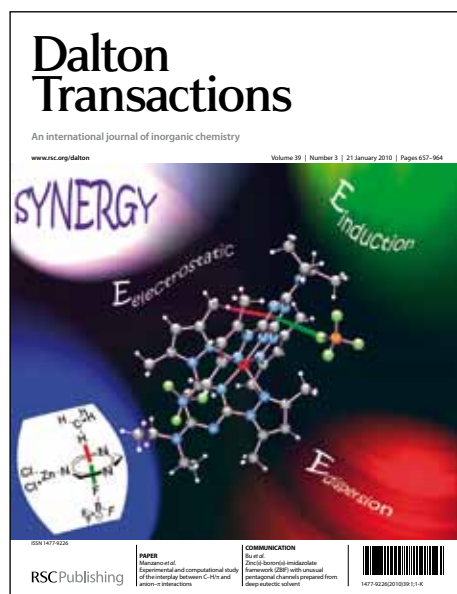


Dalton Transactions

Accepted Manuscript



This is an *Accepted Manuscript*, which has been through the RSC Publishing peer review process and has been accepted for publication.

Accepted Manuscripts are published online shortly after acceptance, which is prior to technical editing, formatting and proof reading. This free service from RSC Publishing allows authors to make their results available to the community, in citable form, before publication of the edited article. This *Accepted Manuscript* will be replaced by the edited and formatted *Advance Article* as soon as this is available.

To cite this manuscript please use its permanent Digital Object Identifier (DOI®), which is identical for all formats of publication.

More information about *Accepted Manuscripts* can be found in the [Information for Authors](#).

Please note that technical editing may introduce minor changes to the text and/or graphics contained in the manuscript submitted by the author(s) which may alter content, and that the standard [Terms & Conditions](#) and the [ethical guidelines](#) that apply to the journal are still applicable. In no event shall the RSC be held responsible for any errors or omissions in these *Accepted Manuscript* manuscripts or any consequences arising from the use of any information contained in them.

Cite this: DOI: 10.1039/c0xx00000x

www.rsc.org/xxxxxx

ARTICLE TYPE

$[\text{IrCl}\{\text{N}(\text{CHCHPr}^t\text{Bu}_2)\}_2]^-$: A versatile source for the Ir^I(PNP) pincer platform.

Markus Kinauer,^a Markus G. Scheibel,^a Josh Abbenseth,^a Frank W. Heinemann,^b Peter Stollberg,^a Christian Würtele,^a and Sven Schneider^{*,a}

Received (in XXX, XXX) Xth XXXXXXXXX 20XX, Accepted Xth XXXXXXXXX 20XX
DOI: 10.1039/b000000x

Reduction of iridium(II) complex $[\text{IrCl}\{\text{N}(\text{CHCHPr}^t\text{Bu}_2)\}_2]$ is reduced by KC_8 to give anionic iridium(I) pincer complex $[\text{IrCl}\{\text{N}(\text{CHCHPr}^t\text{Bu}_2)\}_2]^-$ which was isolated and fully characterized upon stabilization of the counter cation with crown ether as $[\text{K}(15\text{-cr-5})_2][\text{IrCl}\{\text{N}(\text{CHCHPr}^t\text{Bu}_2)\}_2]$. This unprecedented anionic iridium(I) pincer complex completes the unusual, structurally characterized Ir^I/Ir^{II}/Ir^{III} redox series $[\text{IrCl}\{\text{N}(\text{CHCHPr}^t\text{Bu}_2)\}_2]^{-0/+}$, all in square-planar coordination geometry, emphasizing the versatility of this PNP pincer ligand in stabilizing a broad range of oxidation states. The anionic chloro complex is a versatile source for the Ir(PNP) platform. Its reactivity was examined towards chloride ligand substitution against CO and N₂, and oxidative addition of C-electrophiles, C–H bonds and dioxygen, allowing for the isolation of iridium(I) and iridium(III) (PNP) carbonyl, hydrocarbyl and peroxy complexes which were spectroscopically and crystallographically characterized.

Introduction

Pincer ligands have attracted great interest in recent years as rigid, meridionally chelating ligand platforms.^{1,2} In many cases, pincer ligands provide tailorable steric protection around the metal, which proved highly useful for the stabilization of reactive metal fragments in challenging small molecule activation reactions and catalytic transformations, such as alkane dehydrogenation.³ Particularly the ‘archetypical’ anionic PCP ligand $\{\text{C}_6\text{H}_3\text{-2,6-(CH}_2\text{Pr}^t\text{Bu}_2)\}^-$ ($L1^{\text{tBu}}$) was extensively employed. However, besides sterics, the electronic properties have a profound impact on the reactivity, as for example demonstrated for the thermodynamics of C–H oxidative addition.⁴ Particularly, the variation of the central atom of the anionic pincer framework offers strong variation of the donor properties. Hence, the introduction of related anionic pincer ligands with potentially σ -donating donors, such as PNP pincers with diarylamide (Figure 1, $L2$), disilylamide ($L3$), ‘dearomatized’ pyridine based ($L4$) or dialkylamide ($L5$) frameworks are of particular interest.^{5,6,7,8} As for PCP complexes, C–H activation has been studied with some of these ligands, emphasizing the prominent role of transient M(PEP) (E = C, N) with d^8 ions (e.g. M = Rh^I, Ir^I) in T-shaped coordination geometries as pivotal species for facile C–H oxidative addition. Typical pathways for the generation of these reactive intermediates comprise the thermal or photochemical dissociation of small molecules, such as N₂, CO, and olefins⁹ or the reductive elimination of hydrocarbons from M^{III} hydride hydrocarbyl intermediates, e.g. intramolecularly within a cyclometalated complex^{10,11} or by reaction of a dihydrido complex with an alkene

as H₂ acceptor.^{12,13}

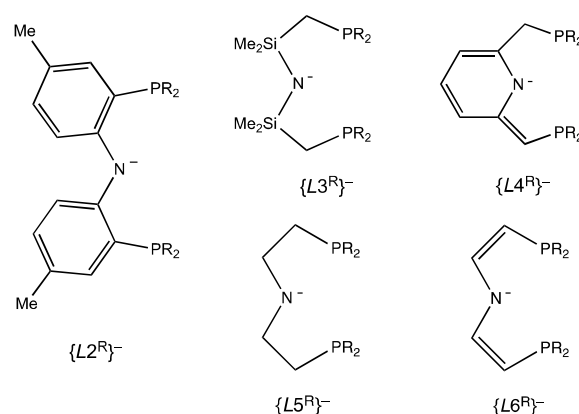
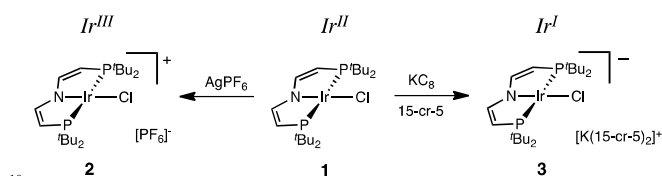


Figure 1. Monoanionic PNP pincer ligands.

Recently, we reported the synthesis of iridium(II) complex $[\text{IrCl}(L6^{\text{tBu}})]$ (**1**, $L6 = \text{N}(\text{CHCHPr}^t\text{Bu}_2)_2$ Scheme 1) by the oxidation of $[\text{IrCl}(\text{H})\text{R}(\text{HL}4^{\text{tBu}})]$ (R = 1-cyclooctenyl) with benzoquinone as hydrogen acceptor.¹⁴ Spectroscopic and computational characterization of **1** indicated the formation of a metal based radical, hence a rare example for a square-planar iridium(II) complex. This dehydrogenative template ligand functionalization provides access to the novel PNP pincer ligand framework $L6$, which represents an aliphatic analogue of $L2$. Notably, in contrast to $L6$ extremely bulky diarylamido PNP ligands, e.g. $t\text{Bu}$ substituted $L2^{\text{tBu}}$, are not synthetically accessible to date. Surprisingly, the characterization of **1** by cyclic voltammetry in CH_2Cl_2 indicated the reversible oxidation to iridium(III) and chemical oxidation with AgPF_6 allowed for the

isolation of first iridium(III) complex with square-planar coordination geometry, $[\text{IrCl}(\text{L6}^{\text{tBu}})]\text{PF}_6$ (**2**). The isolation of such electronically highly unsaturated complexes **1** and **2** enabled the stabilization of extremely rare iridium nitrido complexes $[\text{Ir}(\text{N})(\text{L6}^{\text{tBu}})]^{0/+}$.¹⁵ However, similarly surprising was the observation that electrochemical characterization of **1** under the same conditions also indicated irreversibility of the $\text{Ir}^{\text{I}}/\text{Ir}^{\text{II}}$ reduction wave given that the square-planar coordination geometry is by far predominant for iridium(I).



Scheme 1. Syntheses of the $\text{Ir}^{\text{I}}/\text{Ir}^{\text{II}}/\text{Ir}^{\text{III}}$ redox series **1-3**.

In this paper we describe the isolation and structural characterization of the anionic iridium(I) PNP pincer complex $[\text{K}(\text{15-cr-5})_2][\text{IrCl}(\text{L6}^{\text{tBu}})]$ (**3**) by stabilization of the counter cation with crown ether. This result allows for the comparison of the unusual, isolable $\text{Ir}^{\text{I}}/\text{Ir}^{\text{II}}/\text{Ir}^{\text{III}}$ redox series $[\text{IrCl}(\text{L6}^{\text{tBu}})]^{0/+}$. Complex **3** is a versatile source of the $\text{Ir}(\text{PNP})$ platform as demonstrated by ligand substitution, oxidative addition reactions and C–H and O_2 activation.

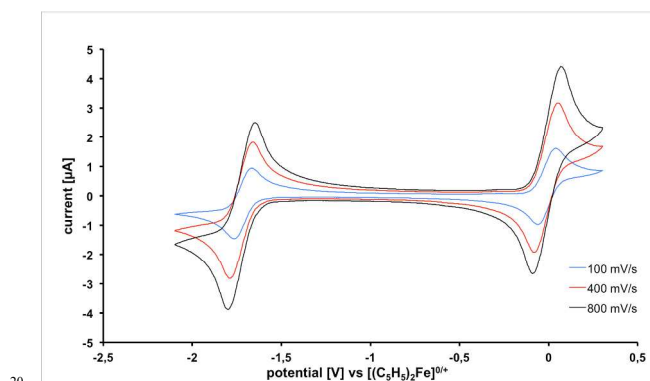


Figure 2. Cyclic voltammogram of **1** in THF (0.1 M $[\text{NnBu}_4][\text{PF}_6]$, room temperature, Pt working electrode) at different scan rates.

Results and Discussion

Anionic iridium(I) pincer complex $[\text{IrCl}(\text{L6}^{\text{tBu}})]^-$

The electrochemistry of **1** was reevaluated by cyclic voltammetry (CV) in tetrahydrofuran (Figure 2). The change of solvent showed for the $\text{Ir}^{\text{I}}/\text{Ir}^{\text{II}}$ redox couple to be reversible even at slow scan rates (10–400 mVs^{-1}) indicating that irreversible reduction of **1** in CH_2Cl_2 might be attributed to reoxidation by the solvent. Accordingly, chemical reduction of **1** with KC_8 in THF and in the presence of crown ether (15-cr-5) affords the isolation of the anionic reduction product $[\text{K}(\text{15-cr-5})_2][\text{IrCl}(\text{L6}^{\text{tBu}})]$ (**3**) in almost 90% yield as an orange compound (Scheme 1). The high air sensitivity of **3** is in line with the low oxidation potential $E_{1/2} = -1.8$ V obtained by CV (Figure 2). Characterization by NMR at room temperature is in agreement with C_{2v} symmetry on the NMR timescale. The ^{31}P chemical shift of **3** exhibits a remarkable

downfield shift by $\Delta\delta = +45$ ppm as compared with the cationic complex **2** indicating a profound influence of the 2-electron reduction on the paramagnetic screening tensor.

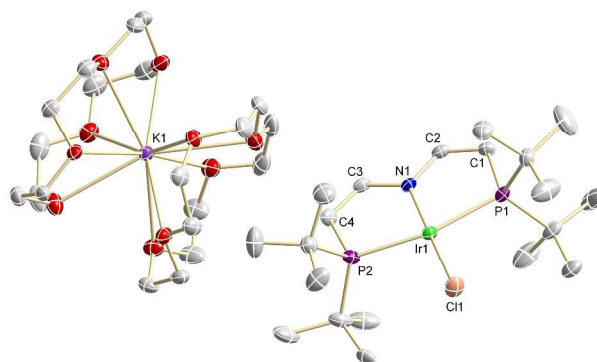


Figure 3. Molecular structure of **3** in the crystal. Selected bond lengths [Å] and angles [°]: Ir1–Cl1 2.3995(8), Ir1–N1 2.030(2), Ir1–P1 2.2779(9), Ir1–P2 2.2760(9), N1–C2 1.370(4), N1–C3 1.369(4), C1–C2 1.349(4), C3–C4 1.350(4); N1–Ir1–Cl1 178.72(7), P1–Ir1–P2 164.00(3).

3 was characterized by single crystal X-ray diffraction (Figure 3) completing a unique, structurally characterized $\text{Ir}^{\text{I}}/\text{Ir}^{\text{II}}/\text{Ir}^{\text{III}}$ redox series (**1-3**) in identical coordination environment. The molecular structure of **3** confirms the distorted square-planar ligand arrangement in the solid state. The distortion arises from the pincer bite angle (P1–Ir1–P2: $164.00(3)^\circ$), which is the smallest within the series (**1**: $166.22(2)^\circ$; **2**: $167.56(2)^\circ$). This trend seems to be a consequence of the strong dependence of the Ir–N bond length on metal oxidation state which is transferred via the rigid pincer ligand backbone. In fact, the Ir–N bond becomes considerably shorter on going from Ir^{I} (2.030(2) Å) to Ir^{II} (1.985(2) Å) and Ir^{III} (1.922(2) Å), respectively.¹⁴ This observation can be most easily rationalized with a simple Lewis structure formalism (Figure 4). As N→Ir π -donation increases with rising metal oxidation state, the Lewis structure **A** (Figure 4) is weighed stronger resulting in a shorter Ir–N distance. Note that the LUMO of **2** has predominant Ir–N π^* -antibonding character, therefore exhibiting considerable Ir–N double bond character.¹⁴ Upon successive reduction to **1** and **3** this orbital will be filled with two electrons resulting in no net Ir–N π -bond in **3**, which provides an MO basis for the observed trend in bond lengths. In turn, the mesomeric Lewis structure **B** exhibits a higher weight upon reduction as reflected in the average pincer backbone N–C (Ir^{I} : 1.37 Å, Ir^{II} : 1.39 Å, Ir^{III} : 1.41 Å) and C–C (Ir^{I} : 1.35 Å, Ir^{II} : 1.34 Å, Ir^{III} : 1.33 Å) bond lengths. However, the effect is much smaller as compared with the Ir–N bond length. Interestingly, the Ir–P bond lengths (**2**: 2.34 Å; **1**: 2.32 Å; **3**: 2.28 Å) exhibit the opposite trend as expected on simple considerations of ionic radii, therefore pointing towards increased Ir→P back donation upon reduction.

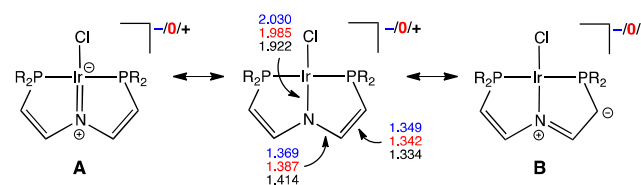
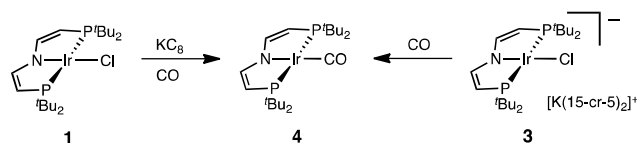


Figure 4. Selected resonance structures and bond lengths for the redox series **3** (Ir^{I} , blue), **1** (Ir^{II} , red), and **2** (Ir^{III} , black).

Hence, the structural parameters within the Ir^I/Ir^{II}/Ir^{III} redox series are in agreement with competitive σ -acceptance of the *N*-lone-pair by the metal centre and the vinyl substituents, respectively, subject to the availability of a vacant (2) or half filled (1) metal *d*-orbital with suitable symmetry. This simple interpretation of the electronic structure explains the stabilization of this unusual redox series by the divinylamido PNP pincer ligand. To our knowledge, the isolation of a [MCl(PEP)]⁻ anion (M = Rh, Ir; PEP = anionic pincer ligand) is unprecedented in pincer chemistry. One related compound, [Ir^I(dippe)₂]⁺ [Ir^ICl₂(dippe)]⁻ (dippe = *i*Pr₂P(CH₂)₂P*i*Pr₂), was previously reported as coordinatively relatively labile intermediate leading to [Ir(□-Cl)(dippe)]₂ and [Ir(dippe)₂]Cl.¹⁶ [Ir(OTf)₂(dfepc)]⁻ (dfepc = (C₂F₅)₂P(CH₂)₂P(C₂F₅)₂) with a highly fluorinated phosphine ligand was also reported, pointing towards stabilization by π -acidic ligands.¹⁷ Accordingly, the dihalodicarbonyl anions of iridium are known for a long time and play an important role in catalytic carbonylation reactions.¹⁸ In our case, the combination of steric protection and electronic flexibility provided by the pincer ligand effectively stabilizes the unusually electron rich anionic complex and the complete Ir^I/Ir^{II}/Ir^{III} redox series.



Scheme 2. Syntheses of carbonyl complex 4.

25 Carbonyl complex [IrCO(L⁶)]

The electronic properties of the Ir(PNP) pincer platform were further probed by the preparation of iridium(I) carbonyl complex [Ir(CO)(L⁶^{tBu})] (4, Scheme 2). 4 can be isolated from direct reduction of 1 with KC₈ under an atmosphere of CO, demonstrating the suitability of the chloride as leaving group. Interestingly, 3 is stable in solution in the absence of CO, yet readily reacts with CO, as well, to give 4. Hence, this observation supports an associative Cl vs. CO substitution mechanism after reduction of 1.

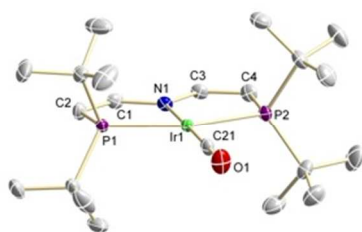
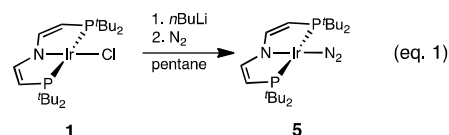


Figure 5. Molecular structure of 4 in the crystal. Selected bond lengths [Å] and angles [°]: Ir1–C21 1.829(2), Ir1–N1 2.061(2), Ir1–P1 2.3137(6), Ir1–P2 2.3080(6), N1–C1 1.367(3), N1–C3 1.371(3), C1–C2 1.347(3), C3–C4 1.351(3), O1–C21 1.153(3); N1–Ir1–C21 178.20(9), P1–Ir1–P2 163.37(2).

The solution NMR data of 4 is in agreement with C_{2v} symmetry. The molecular structure in the solid state was also derived by single-crystal X-ray diffraction (Figure 5) confirming the distorted square-planar coordination geometry around the

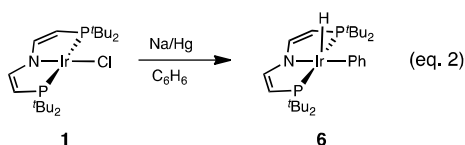
metal centre with a P1–Ir1–P2 bite angle (163.37(2)°) similar to that in 3. Accordingly, the Ir–N distance (2.061(2) Å) is slightly longer as in the case of parent 3 (2.030(2) Å) as a consequence of the higher CO vs. Cl trans-influence, again emphasizing the relationship of pincer bite angle and Ir–N distance within this rigid framework. The CO stretching vibration can be assigned to a signal at 1937 cm⁻¹ in the IR spectrum. This value compares well with the CO band of [Ir(CO)Cl(P*i*Pr₃)₂] (1939 cm⁻¹)¹⁹ or with some corresponding disilylamido ([Ir(CO)(L³^{tBu})]: 1930 cm⁻¹)²⁰ and diarylamido ([Ir(CO)(L²^{iPr})]: 1930 cm⁻¹)²¹ PNP pincer complexes. In contrast, the dialkylamido PNP complex [Ir(CO)(L⁴^{iPr})] exhibits a CO band at considerably lower wavenumber (1908 cm⁻¹),²² emphasizing reduced L→M electron donation by the divinylamido ligand. σ - and π -bonding effects cannot be separated merely from the CO stretching vibration. However, the conjugation of the azallylic C=C double bonds with the *N*-lone pair, which is indicated by the trends within the pincer ligand backbone bond lengths of the Ir^I/Ir^{II}/Ir^{III} redox series (see above) indicates that reduced L→M π -donation of the divinyl- vs. the dialkylamido ligand probably constitutes a significant contribution to the higher of the CO stretching vibration in 3.



Clean reduction of 1 is also accomplished by reaction with *n*BuLi. Monitoring this reaction by ³¹P NMR reveals the quantitative formation of a diamagnetic compound at 56.5 ppm (THF), which was assigned to Li[IrCl(L⁶^{tBu})] by comparison with 3 (55.5 ppm). These solutions were only stable below -20 °C, probably owing to LiCl elimination. However, the Ir(L⁶^{tBu}) fragment could be trapped by thawing a frozen solution under N₂ atmosphere (1 bar) giving [Ir(N₂)(L⁶^{tBu})] (5)¹⁵ in around 60% spectroscopic yield by ³¹P NMR (eq. 1). Hence, the observation of dinitrogen complex 5 suggests that C–H activation reactions should be carried out under argon to avoid inhibition by N₂ binding to the Ir(L⁶^{tBu}) fragment. This observation was also reported for the Ir(L1) platform.^{23,24}

Oxidative addition to [IrCl(L⁶^{tBu})]⁻

Besides substitution for CO, chloride dissociation can also be utilized as source for Ir(L⁶^{tBu}) which undergoes C–H oxidative addition. Reduction of 1 with Na/Hg in benzene results in facile formation of the red iridium(III) hydrido phenyl complex 6 in almost quantitative spectroscopic (³¹P NMR) yield (eq. 2). Isolation of the highly lipophilic compound by crystallization from pentane resulted in isolated yields just below 50%. The addition of benzene to Ir(L⁶^{tBu}) was confirmed by NMR spectroscopy and elemental analysis. The chemical shift of the hydride ligand (δ = -46.5 ppm) suggests a vacant coordination site in *trans*-position, hence the occupation of the apical position within a square-pyramidal coordination geometry around the metal. The three phenyl ¹H and ¹³C signals at room temperature, respectively, indicate rapid rotation around the Ir–C bond on the NMR timescale.



The structural assignments from solution NMR spectroscopy were confirmed by single crystal X-ray diffraction (Figure 6). In the solid state, the five-coordinate metal atom exhibits square pyramidal coordination geometry with the hydride ligand in apical position and an almost linear N–Ir–phenyl bond angle (179.8(3)°). The Ir1–N1 bond (2.109(6) Å) is particularly long due to the strong *trans*-ligand C₆H₅ also resulting in a smaller P1–Ir1–P2 pincer bite angle (162.58(7)°).

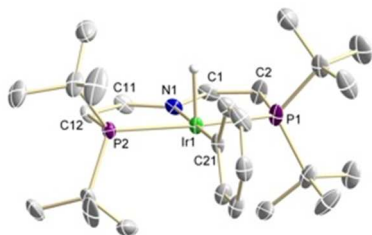
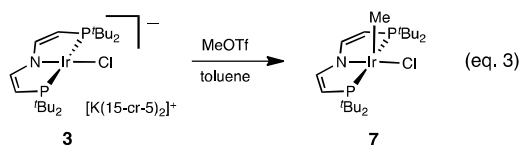


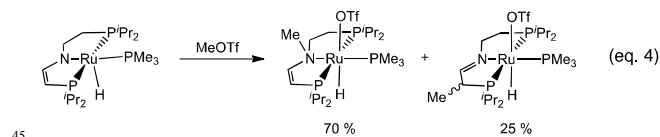
Figure 6. Molecular structure of **6** in the crystal. Selected bond lengths [Å] and angles [°]: Ir1–C21 2.080(7), Ir1–N1 2.109(6), Ir1–P1 2.337(2), Ir1–P2 2.3276(19), N1–C1 1.348(10), N1–C11 1.357(10), C1–C2 1.362(12), C11–C12 1.352(10); N1–Ir1–C21 179.8(3), P1–Ir1–P2 162.58(7).

The C–H oxidative addition most likely proceeds via three-coordinate [Ir(L⁵)] after reduction of **1** and NaCl elimination in the absence of stabilizing crown ether. Such three-coordinate *d*⁸ intermediates are prone to C–H oxidative addition via an intermediate C–H \square -complex.²⁵ However, to our knowledge halides as leaving groups were not previously reported for their formation.



Besides nucleophilic C–H activation, attack of *C*-electrophiles also provides access to iridium(III) hydrocarbyl complexes. The reaction of **3** with MeOTf yields iridium(III) methyl complex [IrCl(CH₃){L⁵^{tBu}}] (**7**) in around 90% yield (eq. 2). Spectroscopic characterization of **7** is in agreement with C_s symmetry on the NMR timescale. The methyl ligand was assigned to signals at 2.08 (1H NMR) and -27.1 ppm (13C NMR), respectively, both exhibiting triplet multiplicity due to coupling with the ³¹P nuclei, unequivocally indicating formation of an iridium(III) methyl complex. In comparison, the dialkyamido complex [Ir(PMe₃){L⁵^{ipr}}] is selectively methylated with MeOTf at the ligand nitrogen atom to form iridium(I) complex [Ir(PMe₃){MeN(CH₂CH₂iPr)₂}]OTf.²⁶ Such ligand centered nucleophilic reactivity was similarly observed for palladium(II) dialkyamido complexes with MeOTf.^{27,28} Also, the five-coordinate alkylvinylamido ruthenium(II) complex [RuH(PMe₃){N(CHCHiPr₂)(CH₂CH₂iPr₂)}] exhibits exclusive ligand methylation upon reaction with MeOTf (eq. 4).²⁹ In this context, the high selectivity of metal alkylation in case of **3** is

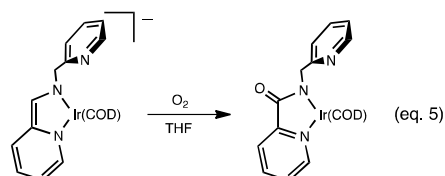
remarkable and emphasizes the rigid, pincer-type behaviour of ligand L₆.



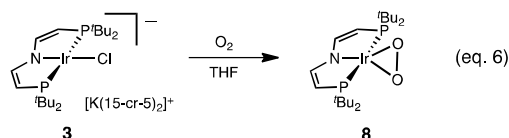
O₂ activation

The activation of dioxygen with iridium complexes has been subject of several studies, e.g. in the context of alkene oxygenation.^{30,31,32} With phosphine pincer ligands, the formation of iridium(III) peroxo complexes, such as [Ir(O₂)(L³^{tBu})] or [Ir(O₂)(L¹^{tBu})], which is in equilibrium with bisdioxygen complex [Ir(O₂)₂(L¹^{tBu})], were reported upon hydrocarbon reductive elimination from iridium(III) under O₂.^{11,33} However, to our knowledge, the only crystallographically characterized iridium pincer mono-O₂ adduct is the ‘POCOP’-complex [Ir(O₂){C₆H₃-2,6-(OPR^{*f*})₂}] (**9**, R^{*f*} = C₆H₂-2,4,6-(CF₃)₃) which was synthesized in the solid state and in turn not spectroscopically examined.³⁴ Hence, a full set of spectroscopic and structural data for this class of compounds is surprisingly not available.

Tejel, De Bruin and co-workers observed the backbone oxygenation of a vinylenediamido ligand instead of cyclooctadiene upon reaction of the corresponding anionic iridium(I) complex with dioxygen (eq. 6).³⁵ Importantly, this reactivity was attributed to the redox non-innocent behaviour of the NNN ligand. Hence, the relationship of this iridate(I) with **3** sparked our interest to examine the reactivity with molecular oxygen.



A solution of **3** in THF immediately turns red upon stirring under dioxygen. From this solution, the oxygen adduct [Ir(O₂)(L₆^{tBu})] (**8**) was isolated as stable compound in around 80% yield (eq. 6). The NMR spectroscopic characterization reveals the formation on a diamagnetic compound with C_{2v} symmetry on the NMR timescale at room temperature. In the IR spectrum a strong band at 910 cm⁻¹ was assigned to the O–O stretching vibration by comparison with parent **3**. This value is at the upper end of the range reported for peroxo ligands and close to the one reported for [Ir(O₂)(L¹^{tBu})] (895 cm⁻¹) suggesting a formal iridium(III) oxidation state for **8**.³⁶ The apparently slightly weaker reducing activation of the dioxygen ligand by the Ir(L₆^{tBu}) compared with the Ir(L¹^{tBu}) fragment is in line with the CO stretching vibrations of **4** (1937 cm⁻¹) vs. [Ir(CO)(L¹^{tBu})] (1913 cm⁻¹).³⁷



The spectroscopic interpretations are corroborated by the molecular structure of **8** (Figure 7). The crystal exhibited disorder with two superimposed positions of the molecule (see ESI). While for this reason the experimental bond lengths and angles should be interpreted with care, some important conclusions regarding O₂ bonding from structural parameters can be drawn. Complex **8** exhibits distorted square-planar geometry and the side-on η²-O₂ ligand occupies the trans-position to nitrogen with perpendicular orientation to this plane. The weak trans-influence of the dioxygen ligand, similar to chloride in **3**, is indicated by the Ir–N distance (2.015(5) Å) and the resulting P–Ir–P bite angle (162.79(4)°). The O–O distance (1.415(7) Å) suggests considerable activation of the dioxygen ligand (*d*_{OO} = 1.21 Å) and is close to the typical range found for Ir(η²-O₂) complexes (1.43–1.53 Å).³⁸ Furthermore, this bond is slightly longer than the ones reported for **9** (1.372(15) Å) and related rhodium dioxygen pincer complexes [Rh(O₂)(L3^{tBu})] (1.363(10) Å) and [Rh(O₂)(L1^{tBu})] (1.365(18) Å; L1^{tBu} = Me₂HC₆(CH₂PtBu₂)₂).^{34,39,40} Hence, the structural features are in agreement with assignment to an iridium(III) peroxo complex, as also indicated by IR spectroscopy. However, as Caulton and co-workers carefully stated about the O–O bond lengths in such η²-O₂ complexes, *perhaps this parameter is not truly reliable for establishing charge state, but rather only the degree of back bonding.*³⁹

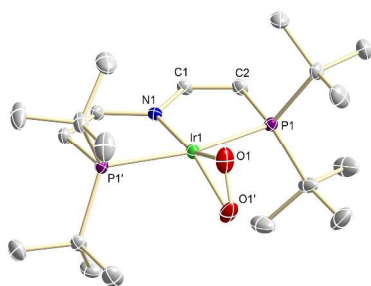


Figure 7. Molecular structure of **8** in the crystal (one of two orientations within the disordered crystal). Selected bond lengths [Å] and angles [°]: Ir1–O1 1.945(3), Ir1–N1 2.015(5), Ir1–P1 2.3461(13), O1–O1' 1.415(7), N1–C1 1.407(4), C1–C2 1.352(5); N1–Ir1–O1 158.66(11), O1–Ir1–O1' 42.7(2), P1–Ir1–P1' 162.79(4).

Experimental Section

General Considerations

All experiments were carried out using Schlenk and glove-box (argon atmosphere) techniques. All solvents were dried by passing through columns packed with activated alumina. Deuterated solvents were obtained from Euriso-Top GmbH, dried over Na/K (C₆D₆ and *d*₈-THF), distilled by trap-to-trap transfer *i. vac.*, and degassed by three freeze-pump-thaw cycles, respectively. C₁₀H₁₀O₅ (Acros), CH₃SO₂CF₃ (Sigma-Aldrich), O₂, H₂ and CO (Linde gas) were used as purchased. Complex **2**, Na/Hg and KC₈ were prepared according to published procedure.^{14,41,42} Elemental analyses were obtained from the Analytical Laboratories at Friedrich-Alexander-University and Georg-August-University, respectively. IR spectra were recorded as nujol mulls between KBr disks on a JASCO FT/IR 4100 Spectrometer. NMR spectra were recorded on a Bruker Avance

III 300 and a Bruker Avance DRX 500 spectrometer and were calibrated to the residual proton resonance of the solvent (C₆D₆: δ_H = 7.16 ppm; δ_C = 128.39; *d*₈-THF: δ_H = 3.58 ppm, 1.72 ppm; δ_C = 67.2 ppm, 25.3 ppm). ³¹P NMR chemical shifts are reported relative to external phosphoric acid (δ = 0.0 ppm). Signal multiplicities are abbreviated as: s (singlet), d (doublet), t (triplet), q (quartet), m (multiplet), br (broad). Cyclic voltammograms were measured on an Autolab PGSTAT101 from Metrohm in a 0.1 M [*n*Bu₄N][PF₆]-solution referenced against the [(C₅Me₅)₂Fe]^{0/+} couple, which was referenced to a potential of -0.440 versus [(C₅H₅)₂Fe]^{0/+}.⁴³

60 Syntheses

[K(C₁₀H₁₀O₅)₂][Ir(Cl){N(CHCHPtBu₂)₂}] (**3**): A mixture of **1** (200.0 mg; 342.4 μmol; 1 eq) and KC₈ (55.5 mg; 410.8 μmol; 1.2 eq) is dissolved in a solution of C₁₀H₁₀O₅ (164.0 μL; 821.7 μmol; 2.4 eq) in THF (15 mL) at □50 °C. After 5 minutes stirring, all volatiles are removed *i. vac.* and the residue is washed with benzene (3 x 5 mL). The crude product is extracted with THF (3 x 7 mL), layered with pentane and crystallized at -32 °C over night. The crystals are collected by filtration, washed with pentane (2 x 5 mL) and dried *i. vac.* **3** is obtained as orange microcrystalline compound (Yield: 164.0 mg; 154.2 μmol; 45%). Anal. Calc. for C₄₀H₈₀ClIrKNO₁₀P₂ (1063.69): C, 45.16; H, 7.58; N, 1.32. Found: C, 44.97; H, 7.60; N, 1.29. NMR (*d*₈-THF, [ppm]): ¹H NMR (300 MHz, 20 °C): δ = 6.93 (ABXX'B'A', N = |²J_{HP} + ⁴J_{HP'}| = 17.2 Hz, ³J_{HH} = 5.2 Hz, 2H, NCHCHP) 4.04 (ABXX'B'A', N = |²J_{HP} + ⁴J_{HP'}| = 4.3 Hz, ³J_{HH} = 5.1 Hz, 2H, NCHCHP), 3.64 (s, 40H, (CH₂CH₂O)₅) 1.35 (A₁₈XX'A'₁₈, N = |³J_{HP} + ⁵J_{HP'}| = 5.9 Hz, 36H, P(C(CH₃)₃)₂). ¹³C NMR (75 MHz, 20 °C): δ = 122.4 (AXX'A', N = |²J_{CP} + ³J_{CP'}| = 5.8 Hz, NCHCHP), 95.0 (AXX'A', N = |¹J_{CP} + ³J_{CP'}| = 22.5 Hz, NCHCHP), 68.6 (s, 20C, (CH₂CH₂O)₅), 38.8 (A₄XX'A'₄, N = |¹J_{CP} + ³J_{CP'}| = 11.2 Hz, 4C, P(C(CH₃)₃), 29.9 (A₆XX'A'₆, N = |²J_{CP} + ³J_{CP'}| = 1.7 Hz, P(C(CH₃)₃). ³¹P NMR (121 MHz, 20 °C): δ = 55.5 (s).

[Ir(CO)₂N(CHCHPtBu₂)₂] (**4**): A mixture of **1** (60.0 mg; 102.7 μmol; 1 eq) and KC₈ (13.9 mg; 102.7 μmol; 1 eq) is dissolved at -50 °C in a THF solution (15 mL) saturated with CO and stirred for 15 min. After removal of all volatiles *i. vac.*, the residue is extracted with pentane (3 x 4 mL) and after evaporation to dryness, the crude product is purified by column chromatography (silanized silica gel, 0.3 x 6 mL, pentane). After removing the solvent *i. vac.*, the product is lyophilized out of benzene (5 mL) and **4** is obtained as bright yellow powder (30.4 mg; 58.9 μmol; 51%). Anal. Calcd. for C₂₁H₄₀IrNOP₂ (576.71): C, 43.73; H, 6.99; N, 2.43. Found: C, 43.82; H, 7.01; N, 2.16. NMR(C₆D₆, [ppm]): ¹H NMR (400 MHz, 21 °C): δ = 7.02 (ABXX'B'A', N = |³J_{HP} + ⁴J_{HP'}| = 18.9 Hz, ³J_{HH} = 5.8 Hz, 2H, NCHCHP), 4.31 (ABXX'B'A', N = |²J_{HP} + ⁴J_{HP'}| = 3.4 Hz, ³J_{HH} = 5.5 Hz, 2H, NCHCHP), 1.36 (A₁₈XX'A'₁₈, N = |³J_{HP} + ⁵J_{HP'}| = 7.0 Hz, P(C(CH₃)₃). ¹³C NMR (100 MHz, 21 °C): δ = 190.6 (t, ²J_{CP} = 7.6, Ir-CO), 163.7 (AXX'A', N = |²J_{CP} + ³J_{CP'}| = 9.6 Hz, NCHCHP), 85.8 (AXX'A', N = |¹J_{CP} + ³J_{CP'}| = 21.5 Hz, NCHCHP), 36.7 (A₂XX'A'₂, N = |¹J_{CP} + ³J_{CP'}| = 13.5 Hz, P(C(CH₃)₃), 29.8 (A₆XX'A'₆, N = |²J_{CP} + ⁴J_{CP'}| = 3.0 Hz, P(C(CH₃)₃). ³¹P NMR (162 MHz, 21 °C): δ = 82.0 (s). IR (cm⁻¹): 1937 vs (ν_{CO}).

Reduction of 1 under N₂ atmosphere: **1** (4.5 mg, 7.7 μmol) is dissolved in pentane (0.5 mL), cooled to □20 °C and *n*-butyllithium (4.8 μL, 1.6 M in *n*-hexane, 7.7 μmol) is added. The solution immediately turns yellow and is cooled to -80 °C. All

volatiles are removed *i. vac.* The residue is dissolved in pentane, and the solution is degassed by three freeze-pump-thaw cycles. After backfilling the vessel with N₂ the mixture is warmed to room temperature and examined by NMR spectroscopy. [Ir(N₂)₂]⁺{N(CHCHPtBu₂)₂}⁻ (**5**), $\delta(^{31}\text{P}) = 70.3$ ppm) is identified as the main product (61%).¹⁵

[Ir(H)(C₆H₅)₂]{N(CHCHPtBu₂)₂} (**6**): A solution of **1** (30.0 mg; 51.4 μmol ; 1 eq) in benzene (5 mL) is added to Na/Hg (1 mol/L; 833.4 mg; 61.6 μmol ; 1.2 eq) and stirred at room temperature for 16 h. The solution is decanted off, the Hg slurry is extracted with benzene (2 x 5 mL) and the combined organic fractions are filtered over a pad of celite. After the removal of all volatiles *i. vac.*, the crude product is extracted with pentane (2 x 5 mL), concentrated and crystallized at -82 °C. The crystals are collected by filtration, washed with cold pentane (3 mL), dissolved in benzene (7 mL) and lyophilized over night. **6** is obtained as red powder (13.0 mg; 21.2 μmol ; 41%). Anal. Calcd. for C₂₆H₄₆IrNP₂ (626.83): C, 49.82; H, 7.40; N, 2.23. Found: C, 49.42; H, 7.25; N, 2.15. NMR(C₆D₆, [ppm]): ¹H NMR (300 MHz, 21 °C): $\delta = 7.73$ (d, ³J_{HH} = 7.5 Hz, 2H, *ortho*-C₆H₅), 7.37 (ABXX'B'A', N = |³J_{HP} + ⁴J_{HP}| = 16.3 Hz, ³J_{HH} = 5.6 Hz, 2H, NCHCHP), 7.20 (m, 2H, *meta*-C₆H₅), 6.97 (t, ³J_{HH} = 7.2 Hz, 1H, *para*-C₆H₅), 4.27 (ABXX'B'A', N = |²J_{HP} + ⁴J_{HP}| = 3.7 Hz, ³J_{HH} = 5.5 Hz, 2H, NCHCHP), 1.14 (A₉XX'A'₉, N = |³J_{AX} + ⁵J_{AX}| = 7.0 Hz, 18H, P(C(CH₃)₃)₂), 1.12 (A₉XX'A'₉, N = |³J_{AX} + ⁵J_{AX}| = 7.0 Hz, 18H, P(C(CH₃)₃)₂), -46.52 (t, ²J_{HP} = 12.6 Hz, 1H, IrH). ¹³C NMR (75.5 MHz, 21 °C): $\delta = 163.6$ (AXX'A', N = |²J_{AX} + ³J_{AX}| = 7.3 Hz, NCHCHP), 144.6 (t, ³J_{CP} = 6.1 Hz, *ortho*-C₆H₅), 128.9 (t, ²J_{CP} = 0.1 Hz, *ipso*-C₆H₅), 127.1 - 126.6 (m, *meta*-C₆H₅), 120.5 (s, *para*-C₆H₅), 85.8 (AXX'A', N = |¹J_{AX} + ³J_{AX}| = 22.6 Hz, NCHCHP), 39.7 (AXX'A', N = |¹J_{AX} + ³J_{AX}| = 12.1 Hz, P(C(CH₃)₃)₂), 35.3 (AXX'A', N = |¹J_{AX} + ³J_{AX}| = 13.4 Hz, PC(CH₃)₃), 29.5 (A₃XX'A'₃, N = |²J_{AX} + ⁴J_{AX}| = 3.0 Hz, PC(CH₃)₃), 29.3 (A₃XX'A'₃, N = |²J_{AX} + ⁴J_{AX}| = 2.7 Hz, PC(CH₃)₃). ³¹P NMR (121.5 MHz, 21 °C): $\delta = 61.3$ (s).

[Ir(Cl)(CH₃)₂]{N(CHCHPtBu₂)₂} (**7**): Methyl triflate (3.7 μL , 33.7 μmol) is added to a solution of **3** (35.4 mg, 33.3 μmol) in toluene (2 mL) at -20 °C and stirred for 5 minutes. After the color of the solution changes from orange to violet, the solution is filtered off and all volatiles are removed *i. vac.* The residue is dissolved in benzene (10 mL), filtered off and lyophilized *i. vac.* overnight. **7** is obtained as analytically pure violet powder (Yield: 10.7 mg; 29.5 μmol ; 89%). Anal. Calc. for C₂₁H₄₃ClIrNP₂ (599.19): C, 42.09; H, 7.23; N, 2.34. Found: C, 42.43; H, 7.06; N, 1.92. NMR(C₆D₆, [ppm]) ¹H NMR (300 MHz, 20 °C): $\delta = 6.82$ (ABXX'B'A', N = |³J_{AX} + ⁴J_{AX}| = 17.8 Hz, ³J_{AB} = 5.8 Hz, 2H, NCHCHP), 4.06 (ABXX'B'A', N = |²J_{BX} + ³J_{BX}| = 3.4 Hz, ³J_{BA} = 6.2 Hz, 2H, NCHCHP), 2.08 (t, ³J_{HP} = 5.3 Hz, 3H, Ir-CH₃), 1.32 (A₉XX'A'₉, N = |³J_{AX} + ⁵J_{AX}| = 6.6 Hz, 18H, P(C(CH₃)₃)₂), 1.24 (A₉XX'A'₉, N = |³J_{AX} + ⁵J_{AX}| = 6.6 Hz, 18H, P(C(CH₃)₃)₂). ¹³C NMR (75 MHz, 20 °C): $\delta = 163.3$ (AXX'A', N = |²J_{AX} + ³J_{AX}| = 7.2 Hz, NCHCHP), 85.3 (AXX'A', N = |¹J_{AX} + ³J_{AX}| = 20.4 Hz, NCHCHP), 40.0 (AXX'A', N = |¹J_{AX} + ³J_{AX}| = 12.1 Hz, P(C(CH₃)₃)₂), 36.2 (AXX'A', N = |¹J_{AX} + ³J_{AX}| = 12.1 Hz, P(C(CH₃)₃)₂), 30.6 (A₃XX'A'₃, N = |²J_{AX} + ³J_{AX}| = 2.2 Hz, P(C(CH₃)₃)₂), 30.0 (A₃XX'A'₃, N = |²J_{AX} + ³J_{AX}| = 2.2 Hz, P(C(CH₃)₃)₂), -27.1 (t, ³J_{CP} = 4.0 Hz, Ir-CH₃). ³¹P NMR (121 MHz, 20 °C): $\delta = 41.9$ (s, P(C(CH₃)₃)₂).

[Ir(O₂){N(CHCHPtBu₂)₂}] (**8**): A solution of **3** (60.0 mg, 56.4 μmol) in 20 mL THF is degassed by one pump-freeze-thaw cycle and the reaction vessel is backfilled with oxygen (1 bar) and stirred at -60 °C for 1h. All volatiles are removed *i. vac.* and the residue is washed with pentane (2 x 5 mL) and extracted with THF (3 x 5 mL) and filtered. The THF solution is layered with pentane (45 mL) and product is crystallized at -32 °C. Red

crystals of **8** are collected by filtration, washed with pentane and dried *i. vac.* (26.3 mg, 45.2 μmol , 80%). Anal. Calcd. for C₂₀H₄₀IrNO₂P₂ (580.71): C, 41.37; H, 6.94; N, 2.41. Found: C, 41.06; H, 6.67; N, 2.23. NMR (*d*₈-THF, [ppm]): ¹H NMR (300 MHz, 20 °C): $\delta = 6.77$ (ABXX'B'A', N = |³J_{HP} + ⁴J_{HP}| = 17.9 Hz, ³J_{HH} = 6.0 Hz, 2H, NCHCHP), 4.76 (ABXX'B'A', N = |²J_{HP} + ⁴J_{HP}| = 4.4 Hz, ³J_{HH} = 6.0 Hz, 2H, NCHCHP), 1.39 (A₁₈XX'A'₁₈, N = |³J_{HP} + ³J_{HP}| = 6.2 Hz, 36H, P(C(CH₃)₃)₂). ¹³C NMR (75.5 MHz, 20 °C): $\delta = 166.9$ (AXX'A', N = |²J_{CP} + ³J_{CP}| = 7.3 Hz, NCHCHP), 98.7 (AXX'A', N = |¹J_{CP} + ³J_{CP}| = 18.7 Hz, NCHCHP), 36.2 (A₂XX'A'₂, N = |¹J_{CP} + ³J_{CP}| = 11.5 Hz, P(C(CH₃)₃)₂), 29.9 (A₆XX'A'₆, N = |²J_{AX} + ⁴J_{AX}| = 3.0 Hz, P(C(CH₃)₃)₂). ³¹P NMR (121 MHz, 20 °C): $\delta = 43.8$ (s, P(C(CH₃)₃)₂). IR (cm⁻¹): 910 s (ν_{OO}).

Crystallographic characterization

Suitable crystals for single crystal X-ray diffraction analysis were selected from the mother liquor under an inert gas atmosphere and transferred in protective perfluoro polyether oil on a microscope slide. Crystals of compound **3** were selected on a microscope slide cooled by a nitrogen gas flow from a X-Temp2 device.^{44,45} The selected and mounted crystals were transferred to the cold gas stream of the diffractometer.

Diffraction data for **3**, **6** and **8** were collected at 100 K with a Bruker D8 three-circle diffractometer equipped with a SMART APEX II CCD detector and an INCOATEC microfocuss source⁴⁶ with Quazar mirror optics ($\lambda = 0.56086$ Å). The data were integrated with SAINT⁴⁷ and a multi-scan absorption correction with SADABS⁴⁸ was applied. The structures were solved by direct methods (SHELXS-2013) and refined against all data by full-matrix least-squares methods on F^2 (SHELXL-2013)^{49,50} within the SHELXLE GUI.⁵¹ The diffraction data for **4** was collected at 150 K with a Bruker-Nonius KappaCCD Diffractometer using MoK α radiation ($\lambda = 0.71073$ Å) and a graphite monochromator. The data were integrated with EvalCCD⁵² and a semi-empirical absorption correction based on multiple scans with SADABS⁵³ was performed. The structure was solved by direct methods and the full-matrix least-squares refinement was carried out on F^2 using SHELXTL NT 6.12.⁵⁴

All non-hydrogen atoms were refined with anisotropic displacement parameters. The C-H hydrogen atoms were refined isotropically on calculated positions by using a riding model with their U_{iso} values constrained to 1.5 U_{eq} of their pivot atoms for terminal sp³ carbon atoms and 1.2 times for all other carbon atoms. The Ir-H hydrogen atom of **6** was located on the electron density map and isotropically refined. The structure of **3** exhibits disorder of one of the CH₃ groups. Two alternative sites were refined with site occupation factors of 0.75 and 0.25, respectively. The disorder of **8** was refined using the PART -1 command and some restraints on the distances and anisotropic displacement parameters (SAME, RIGU).

Conclusions

This study emphasizes the versatility of divinylamido pincer ligand **L6** to stabilize a wide range of oxidation states in identical coordination environments and 1-electron redox-processes within the platinum metals, as demonstrated by an unusual Ir^I/Ir^{II}/Ir^{III} redox series. The bond parameters indicate that the extended π -system within the Ir-N(-C=C)₂ moiety is a decisive electronic feature for the stability of **1-3**. While this ligand platform has similar electronic properties as the popular PNP ligands **L2** and

L3, e.g. expressed in carbonyl stretching vibrations of the corresponding [Ir(CO)(PNP)] complexes, it combines the hydrolytic stability of *L2* (unlike *L3*) with accessibility of the sterically highly protecting phosphine substituents, such as PtBu₂, which are on the other hand not available for *L2*.

The unprecedented anionic iridium(I) chloro pincer complex **3** is an excellent starting material for the synthesis of several iridium(I) and iridium(III) complexes by ligand substitution and oxidative addition. In contrast to [Ir(PMe₃)(L5^{ipr})], exclusively metal-directed oxidative addition of MeOTf is observed, demonstrating the rigid and chemically inert character of the *L6* pincer platform. The use of chloride as leaving group represents a new route to generate the transient M(PEP) (M = d⁸ ion) intermediates, which readily oxidatively add hydrocarbons, like benzene. In reverse, the stabilization of the M(PEP) platform by chloride emphasizes that excess halide salt formation in catalytic transformations could have a detrimental effect on C–H activation with such pincer species, as was observed for N₂. Finally, we presented the first fully spectroscopically and structurally characterized iridium pincer η²-O₂ complex indicating the formation of an iridium(III) peroxo compound.

Acknowledgements

S.S. is grateful to the Deutsche Forschungsgemeinschaft for funding (Emmy Noether Programm SCHN950/2). The authors thank Dr. Regine Herbst-Irmer for help with solving the molecular structure of complex **8**.

Notes and references

^a Georg-August-Universität, Institut für Anorganische Chemie, Tammannstr. 4, 37077 Göttingen, Germany.

^b Department Chemie und Pharmazie, Friedrich-Alexander-Universität Erlangen-Nürnberg, Egerlandstraße 1, 91058 Erlangen, Germany.

E-mail: sven.schneider@chemie.uni-goettingen.de

[†] Electronic Supplementary Information (ESI) available: Crystallographic data (CCDC 967913, 967914, 967915 and 973313). See DOI: 10.1039/c000000x/

- D. Morales-Morales, C. Jensen (Eds.), *The Chemistry of Pincer Compounds*, Elsevier, New York, 2007.
- G. van Koten, D. Milstein (Eds.), *Top. Organomet. Chem.* 2013, **40**.
- J. Choi, A. H. R. MacArthur, M. Brookhart, A. S. Goldman, *Chem. Rev.* 111, **2011**, 1761.
- K. Krogh-Jespersen, M. Czerw, K. Zhu, B. Singh, M. Kanzelberger, N. Darji, P. D. Achord, K. B. Renkema, A. S. Goldman, *J. Am. Chem. Soc.* 2002, **124**, 10797.
- L.-C. Liang, *Coord. Chem. Rev.* 2006, **250**, 1152.
- C. Gunanathan, D. Milstein, *Acc. Chem. Res.* 2011, **44**, 588.
- J. I. Van der Vlugt, J. N. H. Reek, *Angew. Chem. Int. Ed.* 2009, **48**, 8832.
- S. Schneider, J. Meiners, B. Askevold, *Eur. J. Inorg. Chem.* 2012, 412.

- J. Meiners, A. Friedrich, E. Herdtweck, S. Schneider, *Organometallics* 2009, **28**, 6331.
- A. Y. Verat, M. Pink, H. Fan, J. Tomaszewski, K. G. Caulton, *Organometallics* 2008, **27**, 166.
- N. P. Tvetkov, M. F. Laird, H. Fan, M. Pink, K. G. Caulton, *Chem Commun.* 2009, 4578.
- X. Zhang, M. Kanzelberger, T. J. Emge, A. S. Goldman, *J. Am. Chem. Soc.* 2004, **126**, 13192.
- L. Fan, S. Parkin, O. V. Ozerov, *J. Am. Chem. Soc.* 2005, **127**, 16772.
- J. Meiners, M. G. Scheibel, M.-H. Lemée-Cailleau, S. A. Mason, M. B. Boeddinghaus, T. F. Fässler, E. Herdtweck, M. M. Khusniyarov, S. Schneider, *Angew. Chem. Int. Ed.* 2011, **50**, 8184.
- M. G. Scheibel, B. Askevold, F. W. Heinemann, E. J. Reijerse, B. de Bruin, S. Schneider, *Nature Chem.* 2012, **4**, 552.
- S. S. Oster, W. D. Jones, *Polyhedron* 2004, **23**, 2959.
- R. C. Schnabel, D. M. Roddick, *Organometallics* 1996, **15**, 3550.
- M. A. F. Hernandez-Gruel, J. S. J. Pérez-Torrente, M. A. Ciriano, L. A. Oro, *Inorg. Synth.* 2004, **34**, 127.
- R. Meij, D. J. Stufkens, K. Vrieze, W. van Gerresheim, C. H. Stam, *J. Organomet. Chem.* 1979, **164**, 353.
- M. D. Fryzuk, P. A. McNeil, S. J. Rettig, *Organometallics* 1986, **5**, 2469.
- M. T. Whithead, R. H. Grubbs, *J. Am. Chem. Soc.* 2008, **130**, 5874.
- A. Friedrich, R. Ghosh, R. Kolb, E. Herdtweck, S. Schneider, *Organometallics* 2009, **28**, 708.
- D. W. Lee, W. C. Kaska, C. M. Jensen, *Organometallics* 1998, **17**, 1.
- R. Ghosh, M. Kanzelberger, T. J. Emge, G. S. Hall, A. S. Goldman, *Organometallics* 2006, **25**, 5668.
- A. S. Goldman, K. I. Goldberg, in *ACS Symposium Series 885: Activation and Functionalization of C-H Bonds*, ed. K. I. Goldberg, A. S. Goldman, American Chemical Society, Washington, DC, 2004, pp 1-43.
- B. Askevold, A. Friedrich, M. R. Buchner, B. Lewall, A. C. Filippou, E. Herdtweck, S. Schneider, *J. Organomet. Chem.* 2013, **744**, 35.
- S. Park, A. L. Rheingold, D. M. Roundhill, *Organometallics* 1991, **10**, 615.
- A. Marziale, E. Herdtweck, J. Eppinger, S. Schneider, *Inorg. Chem.* 2009, **48**, 3699.
- A. Friedrich, M. Drees, M. Käss, E. Herdtweck, S. Schneider, *Inorg. Chem.*, 2010, **49**, 5482.
- B. de Bruin, P. H. M. Budzelaar and A. W. Gal, *Angew. Chem. Int. Ed.*, 2004, **43**, 4142.
- C. Tejel and M. A. Ciriano, *Top. Organomet. Chem.*, 2007, **22**, 97.
- M. R. Kelley, J.-U. Rohde, *Chem. Commun.* 2012, **48**, 2876.
- D. B. Williams, W. Kaminsky, J. M. Mayer, K. I. Goldberg, *Chem. Commun.* 2008, 4195.
- Z. Huang, P. S. White, M. Brookhart, *Nature* 2010, **465**, 598.
- C. Tejel, M. P. del Río, M. A. Ciriano, E. J. Reijerse, F. Hartl, S. Zális, D. G. H. Hetterscheid, N. Tschlis i Spithas, B. de Bruin, *Chem. Eur. J.* 2009, **15**, 11878.
- J. M. Praetorius, D. P. Allen, R. Wang, J. D. Webb, F. Grein, P. Kennepohl, C. M. Crudden, *J. Am. Chem. Soc.* 2008, **130**, 3724.
- D. W. Lee, C. M. Jensen, D. Morales-Morales, *Organometallics* 2003, **22**, 4744.
- H. Lebel, C. Ladjel, F. Bélanger-Gariépy, F. Schaper, *J. Organomet. Chem.* 2008, **693**, 2645.
- A. Y. Verat, H. Fan, M. Pink, Y.-S. Chen, K. G. Caulton, *Chem. Eur. J.* 2008, **14**, 7680.

-
- 40 C. M. Frech, L. J. W. Shimon, D. Milstein, *Helv. Chim. Acta* 2006, **89**, 1730.
- 41 S. H. Babcock, *Inorg. Synth.* 1939, **1**, 10.
- 42 J.-M. Lalancette, G. Rollin, P. Dumas, *Can. J. Chem.* 1972, **50**, 3058.
- 43 J. R. Aranzaes, M.-C. Daniel, D. Astruc, *Can. J. Chem.* 2006, **84**, 288.
- 44 D. Stalke, *Chem. Soc. Rev.* 1998, **27**, 171.
- 45 T. Kottke, D. Stalke, *J. Appl. Crystallogr.* 1993, **26**, 615.
- 46 T. Schulz, K. Meindl, D. Leusser, D. Stern, J. Graf, C. Michaelsen, M. Ruf, G. M. Sheldrick, D. Stalke, *J. Appl. Crystallogr.* 2009, **42**, 885.
- 47 SAINT 7.68A, Bruker AXS Inst. Inc., WI, USA, Madison, 2009.
- 48 G. M. Sheldrick, SADABS 2012/1, Göttingen, 2012.
- 49 G. M. Sheldrick, *Acta Crystallogr., Sect. A* 2008, **64**, 112.
- 50 P. Müller, R. Herbst-Irmer, A. L. Spek, T. R. Schneider, M. R. Sawaya, In *Crystal Structure Refinement—A Crystallographer's Guide to SHELXL*, IUCr Texts on Crystallography; Müller, P., Ed.; Oxford University Press: Oxford, U.K., 2006; Vol. 8.
- 51 C. B. Hübschle, G. M. Sheldrick, B. Dittrich, B. *J. Appl. Crystallogr.* 2011, **44**, 1281.
- 52 A. J. M. Duisenberg, L. M. J. Kroon-Batenburg, A. M. M. Schreurs, *J. Appl. Cryst.* 2003, **36**, 220.
- 53 SADABS 2.06, Bruker AXS Inc., Madison, WI, USA, 2002.
- 54 SHELXTL NT 6.12, Bruker AXS Inc., Madison, WI, USA, 2002.